Characterizing the size, shape, and compactness of a polydisperse prolate ellipsoidal particle *via* quadruple-detector hydrodynamic chromatography

Amandaa K. Brewer and André M. Striegel*

Received 21st September 2010, Accepted 29th October 2010
DOI: 10.1039/c0an00738b

A detailed quantitative description of particle size, shape, and their distributions is essential for understanding and optimization of the solid-, solution-, and melt-state properties of materials. Here, we employ quadruple-detector hydrodynamic chromatography (HDC) with multi-angle static light scattering, quasi-elastic light scattering, differential viscometry, and differential refractometry detection as a method for characterizing three important physical properties of materials, namely the molar mass, size, and shape of a polydisperse, non-spherical colloidal silica sample. These properties and their distributions were measured continuously across the HDC elution profile of the sample. By combining information from the various parameters determined, we were also able to obtain quantitative knowledge regarding the compactness or denseness of the sample. The applicability of multi-detector HDC to characterize polydisperse, non-spherical analytes was shown to be rapid, accurate, and precise. An advantage over traditional characterization methods is the ability of multi-detector HDC to determine particle size, shape, compactness, and their distributions simultaneously in a single analysis.

Introduction

The processing of raw materials and the end-use properties of products are strongly dependent on particle size and shape. Knowledge of particle geometry is necessary for understanding behaviors such as packing arrangement, sedimentation, mechanical strength, and bulk density of materials.[1–9] Likewise, rheological properties of products and raw materials in fluid mechanical processes such as pumping, mixing, and transport are directly influenced by particle size distribution.[1,5,10,11] As such, a detailed quantitative description of particle size and shape is needed for optimizing the processing and design of both the starting materials and the end products.

Several established techniques such as microscopy, X-ray crystallography, nuclear magnetic resonance (NMR) spectroscopy, and laser diffraction have been previously employed for size and shape characterization of polymers, particles, colloidal aggregates, and micelles,[1–4,11–19] but none have been found fully satisfactory for the determination of both size and shape, and their distributions. For example, microscopy methods only allow for the direct determination of geometric size and shape (but, generally, not their distributions), based on the radius of the smallest circle circumscribing each of the observed particles, as averaged over a fairly limited sample population.[1,12–14,20] Likewise, shape determination from techniques such as X-ray crystallography and NMR involves complex calculations based on the ensemble averages of various combinations of the different Cartesian components of the radius of an object[4,18,19] and provides little information regarding the particle shape distribution.

As seen, particle size and shape analysis is a fairly complex task; to obtain accurate data for both these parameters and their distributions, it is usually necessary to either fractionate or chromatographically separate sample components into essentially monodisperse aliquots prior to detection. Without fractionation or chromatographic separation, the particle size and shape data are generally an average of the overall sample population, uninformative about the individual species present. Because of this, different fractionation and chromatographic techniques, *e.g.*, filtration, sedimentation, field-flow fractionation, size-exclusion chromatography, and hydrodynamic chromatography (HDC), have also been employed for the characterization of polymers, particles, colloidal aggregates, and nanoparticles.[2,11,14,17,21] In the present work we use hydrodynamic chromatography coupled to a train of four detectors, namely multi-angle static light scattering (MALS), quasi-elastic light scattering (QELS), differential viscometry (VISC), and differential refractometry (DRI), to characterize a colloidal silica sample possessing more size heterogeneity and structural complexity than the traditionally studied suspensions of virtually monodisperse spherical latexes.

Hydrodynamic chromatography is a solution-based separation technique which relies on the streamlines of flow in an open tube or in the interstitial volume of a column packed with a non-porous material being preferentially sampled, in a size-dependent manner, by dissolved polymers or particles.[21–28] Separation is due to the parabolic (Poiseuille) flow velocity profile in the open tube channel, which allows small particles to be close to the walls, where the flow is stagnant, while larger particles remain nearer to the center of the tube, where the flow is fastest.[22,23] In HDC, larger analytes elute earlier than smaller ones due to the preferential sampling of the faster streamlines by the larger particles.[21]

In this study, multi-detector hydrodynamic chromatography is introduced as a method for determining the particle size and shape distributions of polydisperse non-spherical analytes. Coupling of the aforementioned detection methods to the

Department of Chemistry & Biochemistry, Florida State University, Tallahassee, Florida, 32306-4390, USA. E-mail: striegel@chem.fsu.edu

separation technique allowed determination of three colloidal radii, the root-mean-square radius or radius of gyration R_G, the hydrodynamic or Stokes radius R_H, and the viscometric radius R_η, as well as the statistical moments and distributions across the HDC elution profile of each of these. The synergistic combination of MALS with either QELS or VISC allowed for the characterization of the analyte based on its shape and compactness as a function of HDC elution volume. Characterization of particle size, shape, and compactness of the sample using multi-detector HDC was achieved in less than twenty minutes.

Experimental

Materials

SNOWTEXT® ST-OUP colloidal silica was obtained from Nissan Chemical America Corporation (Houston, TX, USA). Transmission electron microscopy analysis by the manufacturer indicated a particle diameter between 9 and 15 nm and a particle length between 40 and 100 nm. Sodium azide was obtained from J.T. Baker (Phillipsburg, NJ, USA).

Multi-detector hydrodynamic chromatography (HDC)

Hydrodynamic chromatography analysis was performed on a system consisting of a Waters 2695 separations module with on-line degasser and in-line 0.2 μm nylon filter, connected in series to a DAWN EOS MALS photometer (Wyatt Technology Corp., Santa Barbara, CA, USA), a QELS photometer (Wyatt), a Viscostar differential viscometer (Wyatt), and an Optilab rEX DRI detector (Wyatt), with the MALS and QELS units in the same housing. Separation of unfiltered 100 μL injections occurred over a column bank consisting of two 400 × 7.5 mm PS-1 HDC columns obtained from Agilent/Polymer Laboratories (Amherst, MA, USA), maintained at room temperature. The solvent and mobile phase were deionized H_2O with 0.02% NaN_3, at flow rates of 0.5 and 1.0 mL min^{-1}. Detectors and injection compartment were maintained at 25 °C. For all chromatographic determinations, results are averages of at least four injections, two each from two separate sample dispersions. Data acquisition and processing were performed using Wyatt's ASTRA software (V. 5.3.4.16).

Calibration of the MALS unit was performed by the manufacturer using toluene. Normalization of the MALS unit and interdetector delays and band broadening calculations were performed in-house using a low molar mass (15 000–20 000 g mol^{-1}), narrow dispersity ($M_w/M_n \leq 1.06$) dextran from USB Corporation (Cleveland, OH). All off-line MALS experiments were performed using a Razel model A-99EJ syringe pump to inject a series of seven sample dispersions, ranging from 0.05 to 0.5 mg mL^{-1}, directly into the light scattering photometer, at a flow rate of 0.1 mL min^{-1}. On- and off-line MALS data were fitted using the Zimm model, for data from nine angles ranging from 50° to 126°. (It should be noted that the lowest two angles of the MALS unit are unavailable when the photometer is used as an on-line detector with aqueous eluent. For the remaining angular positions for which scattering is measured in the MALS unit, we discarded data from the two higher-angle photodiodes, from which we were unable to obtain reproducible normalization coefficients, and from two lower-angle photodiodes, which yielded unacceptably low signal-to-noise ratios).

The specific refractive index increment ($\partial n/\partial c$) of the SNOWTEXT® ST-OUP was 0.083 ± 0.002 mL g^{-1}, as determined using the differential refractometer off-line, under the same solvent/temperature/wavelength conditions as above ($\lambda_0 = 685$ nm). The $\partial n/\partial c$ measurement was based on six sample dispersions, ranging from 0.2 to 1.5 mg mL^{-1}, analyzed at a flow rate of 0.1 mL min^{-1}.

Results and discussion

Molar mass

Generally, the most important physical properties for characterizing polymers and particles are molar mass, size, and shape.[4] Because of this, the first physical property we determined was the molar mass of the sample as various processing characteristics, such as flow properties and stiffness, are related to the individual molar mass averages and to the molar mass polydispersity. The molar mass averages of the sample, M_n, M_w, and M_z (Table 1), are calculated *via*:[29–31]

$$M_\beta = \frac{\sum_i c_i M_i^x}{\sum_i c_i M_i^{x-1}} \quad x = 0,\ \beta = n;\ \ x = 1,\ \beta = w;\ \ x = 2,\ \beta = z \tag{1}$$

where, at each elution slice i, c_i is the concentration of the analyte provided by the DRI detector and M_i is the molar mass of the analyte provided by the MALS detector, after correction for interdetector delay. The ratio of the weight-average molar mass M_w to the number-average molar mass M_n, *i.e.*, M_w/M_n, provides a measure of molar mass polydispersity. As seen in Table 1, $M_w/M_n > 1$, indicating that the sample is polydisperse with respect to molar mass. Additional evidence of the molar mass polydispersity of the silica sample is seen in Fig. 1, where M is plotted across the HDC elution profile. From the detector response it appears as if the chromatogram is essentially monomodal; there is only one peak with a shoulder present. If one ignores the poor resolution inherent to HDC,[11] however, and observes rather the molar mass of the analyte as a function of HDC elution volume, it can be seen that there are two species present and that the molar mass of the sample decreases by more than an order-of-magnitude with increasing elution volume, with a small plateau in M at a retention volume of 13.5 mL.

As seen in Table 1, the molar mass averages and polydispersity values of the silica sample do not change when flow rate is changed by a factor of two. From this observation, we conclude that the sample is not experiencing on-column, flow-induced degradation, a feature commonly seen in the analysis of ultra-high molar mass polymers by size-exclusion chromatography[28,32,33] and even, in extreme cases,[28] by HDC. Another indication that the particle is not degrading during analysis comes from the close similarity between the M_w values determined by HDC/MALS and by off-line MALS: the HDC/MALS values obtained at 0.5 and 1.0 mL min^{-1} (Table 1) not only compare quite well to each other, but also to $M_w = 1.44 \pm 0.08 \times 10^7$ g mol^{-1} obtained when the MALS detector was decoupled from the separation system.

Table 1 Ellipsoidal particle molar mass determined by HDC/MALS/QELS/VISC/DRI[a]

Flow rate/mL min^{-1}	M_n/g mol^{-1}	M_w/g mol^{-1}	M_z/g mol^{-1}	M_w/M_n
0.5	1.29×10^7 (0.01×10^7)[b]	1.51×10^7 (0.01×10^7)	2.11×10^7 (0.03×10^7)	1.17 (0.01)
1.0	1.21×10^7 (0.01×10^7)	1.47×10^7 (0.05×10^7)	2.06×10^7 (0.12×10^7)	1.22 (0.06)

[a] In aqueous eluent (see "Experimental") at 25 °C. [b] Values in parentheses correspond to standard deviations.

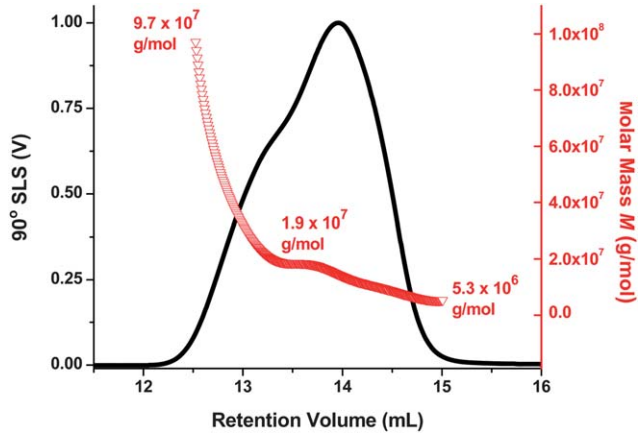

Fig. 1 90° static light scattering (SLS) detector signal, in volts (V), linked to left *y*-axis. Red open triangles represent molar mass, in grams per mole, linked to right *y*-axis.

Particle size

Detailed quantitation of another physical property, particle size, is also achievable with multi-detector HDC. The presence of four physical detection methods permits for the determination of three independent size parameters, a statistical radius and two hard-sphere-equivalent radii. The statistical radius is the radius of gyration or root-mean-square radius R_G, determined using multi-angle static light scattering, which relies on measuring the angular distribution of scattered radiation. The radius of gyration is defined as the root-mean-square distance of an array of atoms from their common center of mass as per:[29,34]

$$R_G = \left[\left(\frac{1}{n+1}\right)\sum_i (r_i - R_{cm})\right]^{1/2} \quad (2)$$

where n is the number of bonds in a particle or polymer, r_i is the location of an individual atom or group of atoms, and R_{cm} is the location of the center of mass of the particle.

The two hard-sphere-equivalent radii, the hydrodynamic radius R_H and viscometric radius R_η, were determined using QELS and a combination of MALS, VISC, and DRI, respectively. The hydrodynamic radius is the radius of an equivalent hard sphere that feels the same force due to flow as does a macromolecule or particle in solution, and is defined as:[29,34]

$$R_H \equiv \frac{k_B T}{6\pi\eta_0 D_T} \quad (3)$$

where k_B is Boltzmann's constant, T is the absolute temperature of the solution, η_0 is the viscosity of the solvent, and D_T is the translational diffusion coefficient of the analyte in solution. The viscometric radius is the radius of a solid sphere that increases the viscosity of the fluid by the same amount as does a macromolecule or particle, and is defined as:[29,34]

$$R_\eta \equiv \left(\frac{3[\eta]M}{10\pi N_A}\right)^{1/3} \quad (4)$$

where $[\eta]$ is the intrinsic viscosity of the analyte solution, M is the analyte molar mass, and N_A is Avogadro's number.

The number-, weight-, and *z*-average values for R_G, R_H, and R_η are given in Table 2. The size polydispersity of the sample can be determined from the polydispersity index ratio (PDI), where PDI is the ratio of the weight- to number-averages of any particular radius. As can be seen in Table 2, all three radii have a PDI > 1. The decrease in R_G, R_H, and R_η as a function of elution volume, seen in Fig. 2, also provides an indication of the size polydispersity present in the sample. The three colloidal radii plotted as a function of HDC elution volume (Fig. 2) follow the same trend as does the molar mass (Fig. 1), with all radii displaying a small plateau around 13.5 mL. Both particle size and molar mass are seen to increase as a function of decreasing elution volume.

As was done with the molar mass, the particle radii were also measured at two different flow rates. As seen in Table 2, all averages of all three radii were essentially flow-rate-independent. Additionally, the $R_{G,z}$ determined by HDC/MALS at both flow rates is virtually identical to the $R_{G,z}$ of 50 ± 1 nm determined by off-line MALS. This collection of results provides ample evidence that the silica particle is not experiencing degradation during HDC analysis.

Table 2 Ellipsoidal particle radii determined by HDC/MALS/QELS/VISC/DRI[a]

Flow rate/mL min^{-1}	$R_{G,n}$/nm	$R_{G,w}$/nm	$R_{G,z}$/nm	$R_{G,w}/R_{G,n}$	$R_{H,n}$/nm	$R_{H,w}$/nm	$R_{H,z}$/nm	$R_{H,w}/R_{H,n}$	$R_{\eta,n}$/nm	$R_{\eta,w}$/nm	$R_{\eta,z}$/nm	$R_{\eta,w}/R_{\eta,n}$
0.5	41 (1)[b]	44 (1)	50 (1)	1.1 (0.1)	23 (1)	25 (1)	28 (1)	1.1 (0.1)	25 (1)	24 (1)	27 (1)	1.1 (0.1)
1.0	39 (1)	43 (1)	48 (1)	1.1 (0.1)	23 (1)	24 (1)	27 (1)	1.1 (0.1)	23 (1)	25 (1)	28 (1)	1.1 (0.1)

[a] In aqueous eluent (see "Experimental") at 25 °C. [b] Values in parentheses correspond to standard deviations.

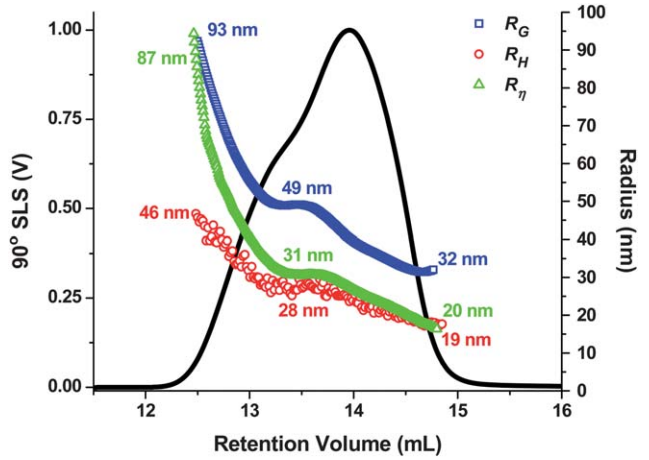

Fig. 2 90° static light scattering (SLS) detector signal, in volts (V), linked to left *y*-axis, and R_G, R_H, and R_η distributions across the elution profile, linked to right *y*-axis. R_G, R_H, and R_η are represented by open blue squares, open red circles, and open green triangles, respectively. Numbers on graph correspond to R_G, R_H, and R_η of analyte at each of the following elution volumes: 12.5, 13.5, and 14.5 mL.

Particle shape

A third physical property which can be determined from multi-detector hydrodynamic chromatography experiments is particle shape. The synergistic coupling of MALS and VISC and MALS and QELS provides two independent dimensionless ratios, $R_{\eta,w}/R_{G,z}$ and $R_{G,z}/R_{H,z}$, respectively, which inform our knowledge of particle shape and compactness. Let us first focus on the ratio $R_{\eta,w}/R_{G,z}$ as a function of HDC elution volume. For our colloidal silica analyte this ratio ranges from 0.94 at the early elution volume, large-radius side of the HDC profile, to 0.62 at the late-elution volume, small-radius side, with a value of 0.63 in the plateau region seen for both molar mass (Fig. 1) and the various radii (Fig. 2). The lower the value of $R_{\eta,w}/R_{G,z}$, the more extended the particle is in solution. The theoretical limit for a hard sphere is $R_{\eta,w}/R_{G,z} = \sqrt{5/3}$, with highly extended structures having an $R_{\eta,w}/R_{G,z}$ value in the range of 0.3–0.4.[35,36] As seen in Fig. 3, the ratio $R_{\eta,w}/R_{G,z}$ decreases as a function of increasing HDC elution volume, indicating that the particle adopts a more extended *conformation* (not to be confused with the particle becoming larger) as both molar mass and size decrease. By combining our knowledge of $R_{\eta,w}/R_{G,z}$, molar mass M, and size across the HDC elution profile we can conclude that the early eluting, larger-sized, high molar mass species are more compact or more dense than the late-eluting, smaller-sized, low molar mass species, which appear to be less compact or dense.

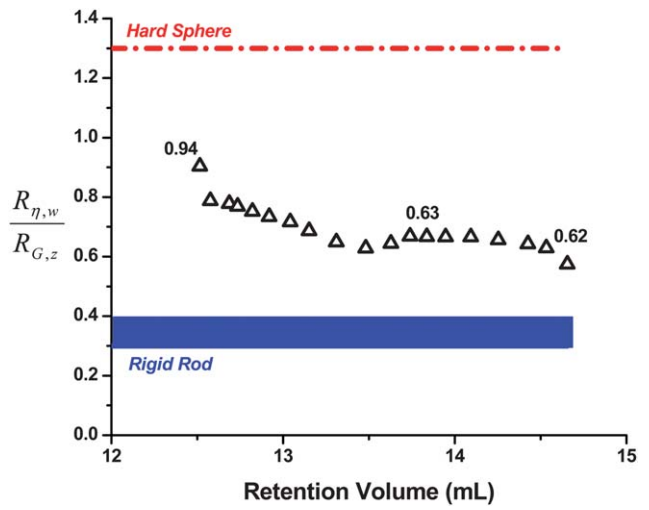

Fig. 3 Change in dimensionless ratio $R_{\eta,w}/R_{G,z}$ as a function of HDC retention volume. Data for sample depicted by black open triangles. Also shown are the hard sphere limit (red dashed-dotted line) and the rigid rod region (in blue).

Information about shape and compactness can also be determined through the ratio of $\rho \equiv R_{G,z}/R_{H,z}$. The theoretical value of ρ is 0.778 for a homogeneous hard sphere and 2.36 for a stiff rod with a molar mass similar to that of the silica sample.[40] The ρ value of ellipsoids with axial ratios between 1 and 100 ranges from 0.875 to 0.987 for oblate ellipsoids, and from 1.36 to 2.24 for prolate ellipsoids.[37–42] The value of ρ for the silica sample examined here decreases from 2.02 to 1.68 as a function of increasing HDC elution volume, a ρ range comparable to that of a prolate ellipsoid. By combining both ratios, $R_{\eta,w}/R_{G,z}$ and ρ, with the molar mass and size data reported above, we can conclude that the composition of the silica sample ranges from large-sized, high-molar mass, compact prolate ellipsoids (which elute early from the HDC columns due to their larger size) to smaller-sized, lower-molar mass, more elongated prolate ellipsoids (the late-eluting species).

The shape of the silica particle was also determined by plotting the experimentally determined $R_{G,z}$ values *versus* the corresponding $R_{H,z}$ values, along with the theoretical predictions of this dependence for spheres, oblate ellipsoids, prolate ellipsoids, and rods, as shown in Fig. 4. Predicted values for spheres and ellipsoids were calculated based on the formulas given in ref. 15,17,38–41 and 43. Results for oblate and prolate ellipsoids were calculated for axial ratios ranging from 1 to 100. For the rigid rod, results were based on the weight-average molar mass of the silica sample. As shown in Fig. 4, the experimental data are in

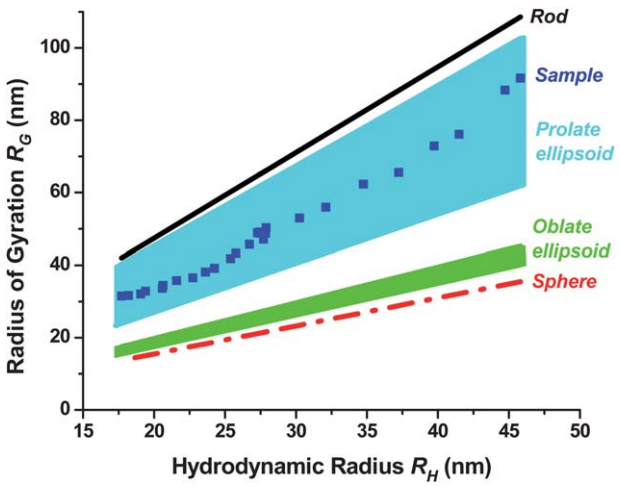

Fig. 4 Radius of gyration (R_G) *versus* hydrodynamic radius (R_H): dark blue squares represent experimental data for the colloidal silica particle; theoretical predictions for spheres, oblate ellipsoids, prolate ellipsoids, and rods are represented by a red dashed dotted line, solid green region, solid light blue region, and solid black line, respectively. The *z*-averages of both radii are plotted in the figure.

good agreement with the predictions for a prolate ellipsoid and lie well above the predicted curves for both oblate ellipsoids and spherical particles. It should also be noted that while the values for the two dimensionless ratios, $R_{\eta,w}/R_{G,z}$ and ρ, both decrease as a function of HDC elution, the slope of the $R_{G,z}$ *versus* $R_{H,z}$ plot is constant and within the range of values of a prolate ellipsoid. This constancy in slope implies that, while the molar mass, size, and compactness or denseness of the analyte all decrease as a function of increasing HDC elution volume, the particle shape remains constant. Finally, by combining the three physical properties discussed here, molar mass, particle size and particle shape, we can conclude that the sample is a polydisperse, prolate ellipsoid spanning the molar mass and size ranges indicated in Fig. 1 and 2, and with molar mass and size averages and polydispersities given in Tables 1 and 2.

Conclusions

A polydisperse, ellipsoidal colloidal silica sample was characterized based on molar mass, size, shape, and their distributions using hydrodynamic chromatography with MALS, QELS, VISC, and DRI detection. All three physical properties were determined as a function of HDC elution volume. The slight bimodality observed in the chromatogram of the sample was evidenced much more strongly by the almost stepwise decrease in both molar mass and size across the HDC elution profile, indicating that the sample is composed of two species of vastly different molar mass and size. By synergistically combining the size information obtained through the use of multiple physical detectors, we were able to also show that, while both species appear to be prolate ellipsoidal particles, the larger, high molar mass species is both more compact (more dense) and more spherical than the smaller, lower molar mass species, which appears to be both less compact (less dense) and more elongated.

The HDC method was shown to be rapid, accurate, and precise. Complete characterization was achieved in less than twenty minutes, and the sample was shown to not have degraded during analysis, as molar mass and size values obtained by HDC/MALS at two different flow rates compared quite well to each other and to values obtained with the MALS detector off-line. Additionally, the size and shape determined using multi-detector HDC compared favorably to those determined by the manufacturer using microscopy. A distinct advantage of multi-detector HDC over other characterization methods is its ability to determine particle size, shape, compactness, and their distributions in a single analysis, using instrumentation common to many polymer separation laboratories.

Acknowledgements

The authors would like to thank Nissan Chemical America Corporation for providing the SNOWTEXT® ST-OUP sample and Agilent/Polymer Laboratories for their kind gift of the HDC columns.

References

1 B. Bujak and M. Bottlinger, *Part. Part. Syst. Charact.*, 2008, **25**, 293–297.
2 M. Baalousha, F. V. D. Kammer, A. Moteclica-Heino and P. Le Coustumer, *Anal. Bioanal. Chem.*, 2005, **383**, 549–554.
3 W. Pabst and C. Berthold, *Part. Part. Syst. Charact.*, 2007, **24**, 458–463.
4 M. Lattuada, H. Wu and M. Morbiedelli, *J. Colloid Interface Sci.*, 2003, **268**, 96–105.
5 C. Servais, R. Jones and I. Roberts, *J. Food Eng.*, 2002, **51**, 201–208.
6 C. I. L. Lee, *J. Paint Technol.*, 1970, **42**, 579–587.
7 D. Colombini, H. Hassander, O. J. Karlsson and F. H. J. Maurer, *Macromolecules*, 2004, **37**, 6865–6873.
8 T. Provder, in *Particle Sizing and Characterization ACS Symposium Series 881*, ed. T. Provder and J. Texter, American Chemical Society, Washington, DC, 2004.
9 H. F. White and S. F. Walton, *J. Am. Ceram. Soc.*, 1937, **20**, 155–166.
10 F. Chu, C. Graillat, J. Guillot and A. Guyot, *Colloid Polym. Sci.*, 1997, **275**, 986–991.
11 A. K. Brewer and A. M. Striegel, *J. Sep. Sci.*, 2010, **33**, 3555–3563.
12 L. F. Pease, D.-H. Tsai, J. L. Hertz, R. A. Zangmeiste, M. R. Zachariah and M. J. Tarlov, *Langmuir*, 2010, **26**, 11384–11390.
13 J. A. Champion, Y. K. Katare and S. Mitragotri, *J. Controlled Release*, 2007, **121**, 3–9.
14 A. K. Brewer and A. M. Striegel, *Anal. Bioanal. Chem.*, DOI: 10.1007/s00216-010-4073-1.
15 C. Y. Young, P. J. Missel, N. A. Mazer and G. B. Benedek, *J. Phys. Chem.*, 1978, **82**, 1375–1378.
16 Y. Han, A. Alsayed, M. Nobili and A. G. Yodh, *Phys. Rev. E: Stat., Nonlinear, Soft Matter Phys.*, 2009, **80**, 011403-1–011403-6.
17 U. Adolphi and W.-M. Kulicke, *Polymer*, 1997, **38**, 1513–1519.
18 L. He and B. Niemeyer, *Biotechnol. Prog.*, 2003, **19**, 544–548.
19 N. Rawat and B. Parbati, *J. Chem. Phys.*, 2009, **131**, 165104-1–165104-9.
20 A. Rawle, *Surf. Coat. Int., Part A*, 2003, **86**, 58–65.
21 A. K. Brewer and A. M. Striegel, *Anal. Bioanal. Chem.*, 2009, **393**, 295–302.
22 H. Small, *J. Colloid Interface Sci.*, 1974, **48**, 147–161.
23 H. Small and M. A. Langhorst, *Anal. Chem.*, 1982, **54**, 892A–898A.
24 D. A. Hoagland, in *Strategies in Size-Exclusion Chromatography. ACS Symposium Series 635*, ed. M. Potschka and P. L. Dubin, American Chemical Society, Washington, DC, 1996, pp. 173–188.
25 J. Bos and R. Tijssen, in *Chromatography in the Petroleum Industry*, ed. E. R. Adlard, Elsevier Scientific, New York, 1995, pp. 95–126.
26 G. Stegeman, J. C. Kraak and H. Poppe, *J. Chromatogr., A*, 1993, **657**, 283–303.
27 A. J. McHugh, in *Size Exclusion Chromatography*, ed. B. J. Hunt and S. R. Holding, Blackie, Glasgow, 1989, pp. 248–270.
28 S. L. Isenberg, A. K. Brewer, G. L. Côté and A. M. Striegel, *Biomacromolecules*, 2010, **11**, 2505–2511.
29 A. M. Striegel, W. W. Yau, J. J. Kirkland and D. D. Bly, *Modern Size-Exclusion Liquid Chromatography*, Wiley, New York, 2nd edn, 2009.
30 A. M. Striegel, *Anal. Chem.*, 2005, **77**, 104A–113A.
31 P. J. Wyatt, *Anal. Chim. Acta*, 1993, **272**, 1–40.
32 A. M. Striegel, S. L. Isenberg and G. L. Côté, *Anal. Bioanal. Chem.*, 2009, **394**, 1887–1893.
33 A. M. Striegel, *J. Liq. Chromatogr. Relat. Technol.*, 2008, **31**, 3105–3114.
34 M. J. Smith, I. A. Haidar and A. M. Striegel, *Analyst*, 2007, **132**, 455–460.
35 J. Roovers, in *Star and Hyperbranched Polymers*, ed. M. K. Mishra and S. Kobayashi, Marcel Dekker, New York, 1999, pp. 285–341.
36 S. G. Ostlund and A. M. Striegel, *Polym. Degrad. Stab.*, 2008, **93**, 1510–1514.
37 M. Antoniette, S. Heinz, M. Schmidt and C. Rosenauer, *Macromolecules*, 1994, **27**, 3276–3281.
38 K. Matsuoka, A. Yonekawa, M. Ishii, C. Honda, K. Endo, Y. Moroi, Y. Abe and T. Tamura, *Colloid Polym. Sci.*, 2006, **285**, 323–330.
39 W. Van De Sande and A. Persoons, *J. Phys. Chem.*, 1985, **89**, 404–409.
40 W. Burchard, in *Advances in Polymer Science 48*, ed. W. Burchard and G. D. Patterson, Springer-Verberg, New York, 1983, pp. 1–124.
41 H. Slayter, J. Loscalzo, P. Bockenstedt and R. I. Handin, *J. Biol. Chem.*, 1985, **260**, 8559–8563.
42 J. Loscalzo, H. Slayter, R. I. Handin and D. Farber, *Biophys. J.*, 1986, **49**, 49–50.
43 P. Wiltzius, *Phys. Rev. Lett.*, 1987, **58**, 710–713.